Journal of Photoscience, Vol. 6, No. 3, pp. 91 – 96

ARTIFICIAL PHOTOSYNTHESIS USING ZEOLITES

NORMA B. CASTAGNOLA AND PRABIR K. DUTTA*
Department of Chemistry, The Ohio State University, Columbus, OH43210, USA

(*Received* 28 *June* 1999; *accepted* 30 *July* 1999)

Abstract – Zeolites and microporous materials continue to attract attention as novel hosts for photochemical reactions. Zeolites are attractive because of their ability to selectively exchange and incorporate species within the void spaces and interconnecting channels, providing a spatial arrangement of molecules. Our research has primarily focused on intrazeolitic electron transfer from excited $Ru(bpy)_3^{2+}$ in supercages of zeolite Y to a series of bipyridinium ions. In the $Ru(bpy)_3^{2+}$- viologen-zeolite Y samples, the slowing of the back electron transfer from the bipyridinium radical cation to $Ru(bpy)_3^{3+}$ allows for charge propagation *via* self exchange between diquat molecules. This provides an opportunity for permanent charge separation. When the migrating charge on the diquat radical within the zeolite reaches the surface, it can be transferred to a neutral viologen (PVS) in solution, resulting in permanent charge separation. The advantage of long-lived charge separation can be exploited for useful chemistry if suitable catalysts can be assembled on the zeolites. We have studied RuO_2 as water oxidation catalysts. We have demonstrated that synthesis of RuO_2 fibers on a zeolite via thermal decomposition of $Ru_3(CO)_{12}$ leads to the most active water decomposition catalyst reported to date. Because of the extensive interest of photochemical water reduction to H_2, much is known about catalytic systems using one electron reduced viologen species as reactants, and it has been reported that RuO_2/zeolite is an effective water reduction catalyst, and even more importantly, that no reaction of viologen occurred with H_2 over this catalyst. The present challenge is to incorporate all these elements of the system into an architecture and we are examining zeolite membranes for this purpose.

INTRODUCTION

Photosynthesis involves the conversion of energy from sunlight to chemicals, and is responsible for maintaining all living organisms on earth.[1] By designing systems that mimic photosynthesis, sunlight reaching the earth's surface can be exploited to generate useful chemicals.[1,2] In order to realize this objective, a system that absorbs light over a broad spectrum of wavelengths and uses these photons efficiently to generate long-lived energetic charge separated states is necessary.[3] In addition, the photogenerated redox species need to be capable of doing useful chemistry. This process can be schematically represented by Scheme 1.

Scheme 1.

In photosynthesis, nature accomplishes these objectives by a complex array of light harvesting pigments and redox species in proteins that are arranged in a definite spatial manner across membranes.[1] From a chemical viewpoint, three basic phenomena control the use of light energy: energy capture, transfer, and photoinitiated electron transfer. In constructing artificial photosynthetic assemblies, our aim is to optimize the photochemical electron transfer represented by Scheme 2.

$$D \xrightarrow{h\nu} D^*$$
$$D^*+A \longrightarrow D^+ + A^-$$

Scheme 2.

where D is a sensitizer donor molecule excited by absorption of visible light. This makes it a better reducing agent, and can reduce an acceptor species A. If the redox properties of D^+ and A^- are such that they can do useful chemistry, such as splitting water into hydrogen and oxygen, then a light driven process for generation of fuels becomes possible. Other useful reactions include conversion of CO_2 into methane or methanol, or the conversion of nitrogen into ammonia[2]. For Scheme 2 to become practical, several conditions need to be satisfied. First, D must be chosen for optimum absorption of sunlight, and the excited state lifetime of D^* has to be long-lived for reaction with A. Second, following electron transfer, D^+ and A^- need to be separated from each other so that the favorable (yet wasteful) back electron transfer reaction $D^+ + A^- \rightarrow D + A$ can be minimized. Third, these photochemically generated redox species need to be accessible. Finally, the system will need to return to its initial state such that the photochemical cycle can continue. Since photo-

*To whom correspondence should be addressed.

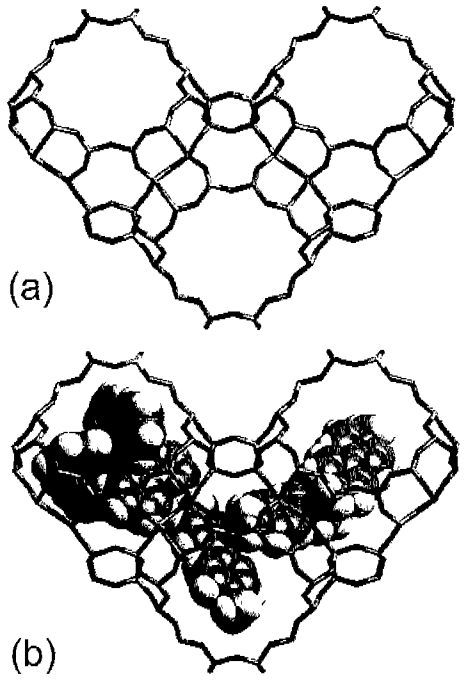

Figure 1. (a) A cross-sectional view of three supercages of zeolite Y. (b) The photochemical system $Ru(bpy)_3^{2+}$ (left cage) and methylviologen packing in the zeolite cages.

splitting of H_2O involves multi-electron steps, whereas in Scheme 2 only single electron-transfer reactions are occurring, appropriate chemistries for the electrons to be collected and coupled to a multi-electron process are necessary.

In this context, it is becoming increasingly clear that microheterogeneous supports provide a novel way to arrange molecules in space and also have the potential to build in other functional requirements of a practical system, such as catalysts.[4] In this paper, we report the progress our group has made in this area using zeolites as hosts for assembly of an artificial photosynthetic unit.

RESULTS AND DISCUSSION

I. Zeolite-Based Assemblies

Zeolites are crystalline aluminosilicates with chemical composition represented by the formula $M_{2/n}O \cdot Al_2O_3 \cdot xSiO_2 \cdot yH_2O$.[5] The three dimensional structure is made up of corner sharing SiO_4 and AlO_4 tetrahedra, with the cations M^{n+} occupying extraframework positions and balancing the charge of the AlO_4 unit of the framework.[5] Interconnecting cages and channels make up the internal structure of zeolites.

The dimensions of the cages and channels in zeolites vary from 2 to 13 Å and extend in a regular fashion throughout a typical ~100,000 Å zeolite crystal. This internal architecture of zeolites allows for novel spatial arrangement of molecules. Fig. 1a shows three supercages of a zeolite Y, the framework of interest in this study.

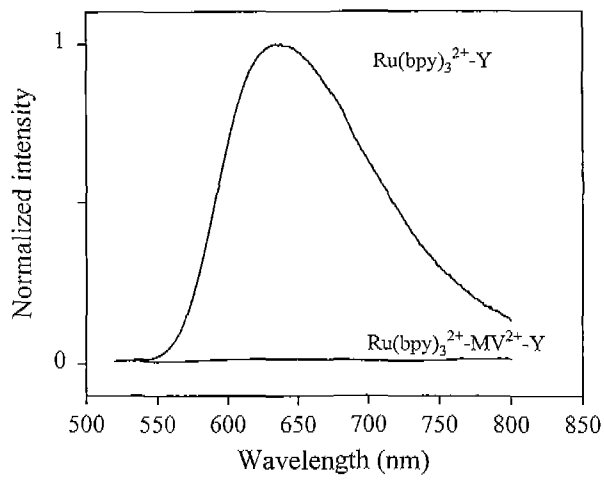

Figure 2. Emission of $Ru(bpy)_3^{2+}$- zeolite Y and $Ru(bpy)_3^{2+}$-MV^{2+}- zeolite Y.

A. Photochemical System

Our efforts for the photochemical splitting of water involves the following scheme:

$$Ru(bpy)_3^{2+} \longrightarrow Ru(bpy)_3^{2+*}$$
$$Ru(bpy)_3^{2+*} + MV^{2+} \longrightarrow Ru(bpy)_3^{3+} + MV^{+\cdot}$$
$$4Ru(bpy)_3^{3+} + 2H_2O \longrightarrow 4Ru(bpy)_3^{2+} + 4H^+ + O_2$$
$$2MV^{+\cdot} + 2H^+ \longrightarrow 2MV^{2+} + H_2$$

Scheme 3.

The forward electron transfer from the photoexcited $Ru(bpy)_3^{2+}$ to viologen is very facile, with a diffusion controlled rate constant of 2.5×10^9 $M^{-1}sec^{-1}$.[6] However, the back electron transfer is also very fast and the challenge is to design a system in which the back electron transfer from the viologen cation radical $MV^{+\cdot}$ to $Ru(bpy)_3^{3+}$ can be slowed down or even prevented.

The strategy we followed was to encapsulate $Ru(bpy)_3^{2+}$ in the zeolite supercage, and examine electron transfer to viologens in neighboring supercages as shown by the scheme in Fig. 1b. The synthesis of $Ru(bpy)_3^{2+}$ within the supercages of zeolite-Y was first reported by Quayle and Lunsford almost two decades ago.[7]

Once synthesized within the zeolite, $Ru(bpy)_3^{2+}$ is essentially trapped. The complex has a diameter of 12.1 Å, fitting snugly within the 13 Å supercage but unable to move through the 7 Å windows. Since the occupied supercage is essentially filled by the $Ru(bpy)_3^{2+}$ complex, the closest approach available to a viologen is in an adjacent supercage as shown in Fig. 1b.

B. Forward electron transfer

Fluorescence of zeolite-entrapped $Ru(bpy)_3^{2+}$ was measured

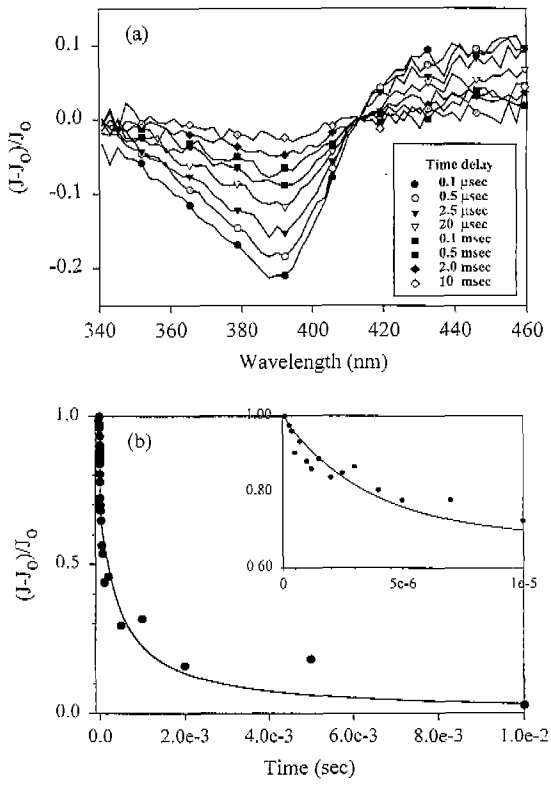

Figure 3. (a) Decay of the absorption due to $MV^{+\cdot}$ as a function of time, as measured by time resolved diffuse reflectance spectroscopy. (b) Plot of the intensity at 390 nm as a function of time and the fit using the model explained in the text.

in the absence and presence of MV^{2+}, and the data shown in Fig. 2. The loading of the chromophore is 1 Ru per 15 supercages, and for MV^{2+} the loading is 1 molecule per supercage. When $Ru(bpy)_3^{2+}$ and methyl viologen are in neighboring supercages, oxidative quenching of $Ru(bpy)_3^{2+*}$, as exemplified below, can occur:

$$Ru(bpy)_3^{2+*} + MV^{2+} \text{ (next cage)} \xrightarrow{k_f} Ru(bpy)_3^{3+} + MV^{+\cdot}$$

The efficiency of the forward electron transfer is reflected in the fluorescence quenching. A rate constant of $7.9 \times 10^7\ s^{-1}$ for the $Ru(bpy)_3^{2+}$-MV^{2+} system was estimated using the following equation:

$$k_f = (I_o/I - 1)/\tau_d$$

where I_o and I correspond to the emission intensity of $Ru(bpY)_3^{2+*}$ in the absence and presence of the quencher and τ_d is the experimental lifetime of the unquenched $Ru(bpy)_3^{2+*}$-Y. From the emission decay monitored at 610 nm, the lifetime determined was 620 ns.

C. Back electron transfer

The dynamics of the back electron transfer were obtained by monitoring the decay of the bipyridinium radical signal

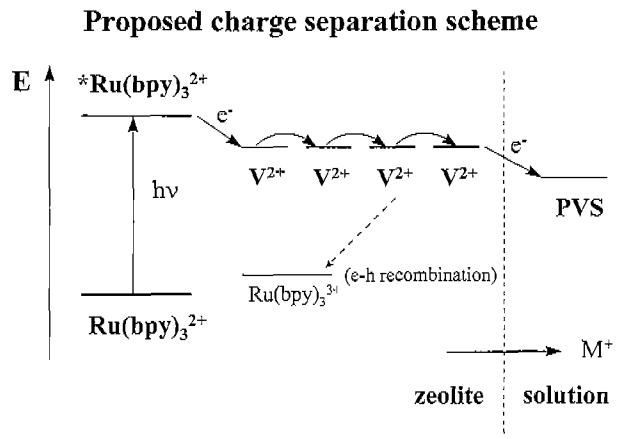

Figure 4. Model for a zeolite based ternary system for permanent charge separation.

as a function of time. Fig. 3a shows the intensity of the $MV^{+\cdot}$ signal at various times after the electron transfer initiating laser pulse. Fig. 3b plots the intensity at 389 nm as a function of time, and does not follow a monoexponential decay.

A more complicated model was developed to describe the decay behavior of the high loading samples.[8] In addition to the back electron transfer reaction,

$$MV^{+\cdot} + Ru(bpy)_3^{3+} \xrightarrow{k_b} MV^{2+} + Ru(bpy)_3^{2+}$$

we needed to include the following additional reactions:

$$MV^{+\cdot} + MV^{2+} \xrightarrow{k_{hop}} MV^{2+} + MV^{+\cdot}$$

$$Ru(bpy)_3^{3+} + MV^{+\cdot} \xrightarrow{k_2} Ru(bpy)_3^{2+} + MV^{2+}$$

Electron hopping between bipyridinium ions (khop) provides a pathway for the electron to move farther away from the $Ru(bpy)_3^{3-}$ center. Once the electron has hopped on to neighboring cages, it can "diffuse" around in the zeolite via charge hopping until it encounters a $Ru(bpy)_3^{3+}$.

This recomb ination process is control led by k_2, a second order rate consta nt. The solid line in Fig. 3b is the model that simulat es the experi mental data and it was obtaine d with the rate consta nts k_b, k_{hop} and k_2 of $9.0 \times 10^{4}\ s^{-1}$, $2.0 \times 10^5\ s^{-1}$ and $3.0 \times 10^3\ conc^{-1}s^{-1}$, respectively.

This kinetic model can then adequately explain permanent charge separation that Borja and Dutta reported on a ternary system.[9] The intrazeolitic electron transfer was between encapsulated $Ru(bpy)_3^{2+}$ and N,N′-tetramethylene-2,2′-bipyridinium ion (DQ^{2+}) of reduction potential $E^o = -0.65$ V. Upon oxidative quenching of the excited $Ru(bpy)_3^{2+*}$, the reduced $DQ^{+\cdot}$ was then capable of transferring the electron to a second, zwitterionic neutral viologen (propylviologen sulfonate, $E^o = -0.41$V, PVS) of lower potential present in the surrounding solution. This ternary system is illustrated in Fig. 4. Visible photolysis (200 mW of 400-600 nm light) results in the generation of the blue anion radical $PVS^{-\cdot}$ in solution. Charges that migrate onto the zeolite surface can be transferred to

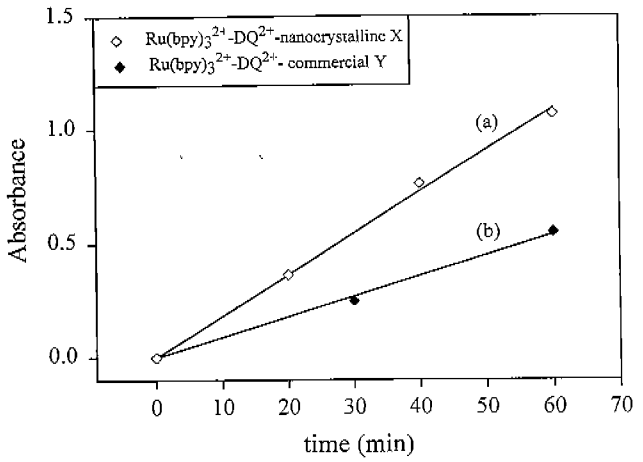

Figure 5. Comparison of the PVS radical yield with (a) nanocrystalline and (b) conventional micron-sized zeolite Y.

PVS in solution, resulting in permanent charge separation:

$$\{Ru(bpy)_3^{2+}...DQ^{2+}\}_z \xrightarrow{h\nu} \{Ru(bpy)_3^{2+*}...DQ^{2+}\}_z$$

$$\{Ru(bpy)_3^{2+*}...DQ^{2+}\}_z \xrightarrow{k_f} \{Ru(bpy)_3^{3+}...DQ^{+\cdot}\}_z$$

$$\{Ru(bpy)_3^{3+}...DQ^{+\cdot}\}_z \xrightarrow{k_b} \{Ru(bpy)_3^{2+}...DQ^{2+}\}_z$$

$$\{Ru(bpy)_3^{3+}...DQ^{+\cdot}\}_z + PVS_s \xrightarrow{k_s} \{Ru(bpy)_3^{3+}...DQ^{2+}\}_z + PVS_s^{-\cdot}$$

where z represents the zeolite and s the solution. Measurement of the reduced viologen ($PVS^{-\cdot}$) in solution by UV-visible spectroscopy provides a good measure of the charge separation efficiency. Recently, Sykora and Kincaid have used the same strategy to improve further the photochemical yield.[10]

Considering that the charge transfer from the zeolite to the PVS in solution is taking place at the zeolite-solution interface, nanocrystallites should result in higher photochemical yields as compared to regular micron-sized crystallites, based on the higher surface-to-volume ratios. Fig. 5 shows the results of a typical photolysis experiment for $Ru(bpy)_3^{2+}$-nanocrystalline X and conventional micron-sized $Ru(bpy)_3^{2+}$-zeolite Y crystallites, which shows that the growth of PVS-. radical (390, 620 nm) in solution as a function of photolysis time is a factor of two improvement in the nanocrystalline zeolite.[11]

However, because of the extensive aggregation in nanocrystalline zeolites, the full advantage of the reduction in crystallite size could not be achieved. Comparison of surface-to-volume ratios for 250 nm aggregates with the 1 μm crystals suggest that a four-fold improvement is expected. It is clear that if well-dispersed $Ru(bpy)_3^{2+}$ containing nanocrystallites can be synthesized, use of the sensitizer-donor strategy described here will lead to significant improvements in photochemical charge separation. This is currently being pursued.

II. Development of Catalysts

Incorporating $Ru(bpy)_3^{2+}$ and viologens into zeolites provide opportunities for long-lived charge separation. Utilization of these charge-separated species requires the presence of catalysts.

Oxygen Evolution Catalysts

Several years ago Lehn and coworkers reported that RuO_x and IrO_x deposited on zeolite Y were very efficient catalysts for the oxidation of water to O_2 by $Ru(bpy)_3^{3+}$.[12,14] The photochemical process involved the following scheme:

$$Ru(bpy)_3^{2+*} + [Co(NH_3)_5Cl]^{2+} \longrightarrow Ru(bpy)_3^{3+} + [Co(NH_3)_5Cl]^{+}$$

$$[Co(NH_3)_5Cl]^{+} + 5H^{+} \longrightarrow Co^{2+}(aq) + 5NH_4^{+} + Cl^{-}$$

Photochemically excited $Ru(bpy)_3^{2+*}$ reduces the complex $[Co(NH_3)_5Cl]^{2+}$. The back electron transfer from $[Co(NH_3)_5Cl]^{+}$ was thwarted because of the decomposition of $[Co(NH_3)_5Cl]^{+}$ to Co^{2+}, NH_4^{+} and Cl^{-}, thus forming long-lived $Ru(bpy)_3^{3+}$. The activity of ruthenium and iridium oxides as catalysts is consistent with the fact that these materials have the smallest overpotentials for oxygen evolution when used as anodic materials in water electrolysis.

We have reported an alternate method to make RuO_x-zeolite Y catalysts.[13] An intimate mixture of $Ru_3(CO)_{12}$ and zeo-

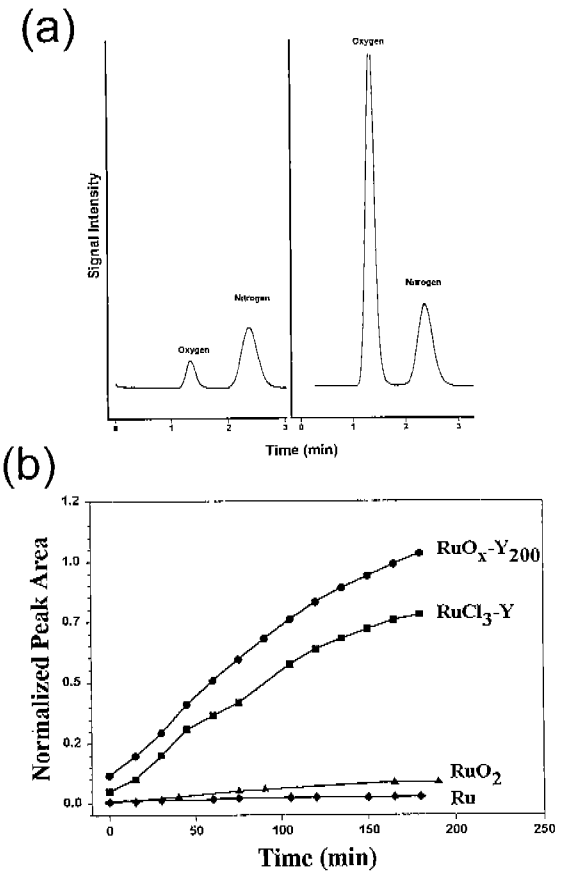

Figure 6. (a) GC of headspace of $Ru(bpy)_3^{3+}$ reaction with water before (left) and after photolysis (right) using RuO_x-zeolite Y as catalyst. (b) Comparison of oxygen evolution using a series of Ru based catalysts.

lite Y was heated under vacuum to 170°C for 5 hours. Based on the thermal decarbonylation of $Ru_3(CO)_{12}$ on silica, the following steps are expected to occur:

$$Ru_3(CO)_{12} \rightarrow Ru_3(CO)_8 \rightarrow Ru_3(CO)_5 \rightarrow Ru$$

Upon continued heat treatment in air at higher temperatures, powder X-ray diffraction indicates the formation of RuO_x on the zeolite. This material was examined as a catalyst for photodecomposition of water to oxygen by the following reaction:

$$4Ru(bpy)_3^{3+} + 2H_2O \xrightarrow{RuO_2/zeolite} 4H^+ + O_2 + 4Ru(bpy)_3^{2+}$$

Fig. 6a compares the GC trace of the headspace before and after two hours of photolysis using the catalyst RuO_2-zeolite Y obtained by aerobic heat treatment of Ru-Y at 200°C (RuO_2Y_{200}). Because the catalyst amounts, solution concentrations and the conditions of photolysis remain unchanged, the measure of the oxygen peak areas in the GC provide a quantitative estimate of the catalytic activity.

Fig. 6b compares the catalytic activity of the sample generated by air oxidation at 200°C (RuO_2Y_{200}) with a sample generated by oxidation of $RuCl_3$ on zeolite Y[14] and commercial RuO_2 powder and metallic Ru. The RuO_2 catalyst obtained by air oxidation at 200°C outperforms the other catalysts.

III. Proposed Development of a Membrane-Based System

The water oxidation reported above was carried out with $Ru(bpy)_3^{3+}$ generated photochemically with sacrificial electron donors and the RuO_2/zeolite. The challenge now is to develop an architecture where the intrazeolitic $Ru(bpy)_3^{3+}$ and viologen radical can be used simultaneously without the need for sacrificial electron donors. As we have reported above, the viologen radical can be transferred from the zeolite into solution via an interfacial zeolite-solution electron transfer. Based on the literature, it appears that this viologen radical in solution can be coupled with the RuO_2/zeolite catalyst to produce H_2.[15] The problem with this architecture is to access the $Ru(bpy)_3^{3+}$ which is trapped in the supercages of the zeolite.

Clearly, a new strategy is required. Most importantly, the O_2 generated by $Ru(bpy)_3^{3+}$ *via* a catalyst has to be kept separated from the viologen radicals. We propose here the utilization of a zeolite membrane to solve this problem. Considerable research has been done over the past decade on zeolitic membranes.[16] What is needed for this project is a channel zeolite in which all the crystallites are oriented with the channels all approximately aligned along the membrane axis. There is an example of such a zeolite membrane in the literature. Anderson and coworkers have reported in a communication in 1992 that gmelinite membranes with a high degree of crystal ordering can be synthesized.[17] Gmelinite is an excellent choice for a framework since it has channels of the 7 Å that can readily fit viologen (diquat) molecules and has a Si/Al ratio of 3, which indicates that it has reasonably large ion-exchange capacity, necessary for packing of viologen ions.

The important aspects of such a system are:

(a) **Slow back electron transfer.** This is possible because of the constrained motional freedom of the Ru(polypyridyl) moiety. Mallouk and coworkers have reported that the incorporation of covalently linked structures on a zeolite surface leads to lowering of the back electron transfer reaction.[18]

(b) **Fast forward reaction.** By choosing the two bpy ligands on the Ru to be more difficult to reduce than the bpy attached to the viologen, forward electron transfer to the viologen is promoted. Elliott and coworkers have documented the electron transfer in these systems.[19]

(c) **Propagation of charge by self-exchange.** By having the channels packed with $2DQ^{2+}$ or MV^{2+}, we expect efficient charge transport by self-exchange.

(d) **H_2 evolution.** Viologen radicals formed within the zeolite can interact with RuO_2 on the zeolite surface to produce H_2.

(e) O_2 evolution. Since contact of $Ru(bpy)_3^{3+}$ with RuO_2 is necessary for water oxidation and $Ru(bpy)_3^{2+*}$ is possibly quenched by RuO_2, we will suspend the RuO_2/zeolite Y as nanocrystallites in solution. This will resemble the $Ru(bpy)_3^{2+}$ (solution) - RuO_2 (zeolite Y) reported above, in which efficient O_2 evolution was observed.

Based on this strategy, we are presently assembling a zeolite-based photochemical water splitting system.

Acknowledgments–We acknowledge funding by the Department of Energy, Basic Sciences Division.

REFERENCES

1. Lawlor, D.W. (1993) *Photosynthesis: Molecular, Physiological and Environmental Processes*, 2nd ed., Longman, Essex. (b) Govindjee, E. (1982) *Energy Conversion by Plants and Bacteria*. Academic, New York.
2. Parmon, V.N. and K.I. Zamarev (1989) *Photocatalysis: Fundamentals and Applications*, N. Serpone and E. Pelizzetti, Eds., Wiley, New York, pp. 565-602.
3. Kalyanasundaram, K. (1987) *Photochemistry in Microheterogeneous Systems*, Academic, New York.
4. (a) M. Grätzel, Ed. (1983) *Energy Resources Through Photochemistry and Catalysis*, Academic, New York. (b) Ramamurthy, V. (1991) *Photochemistry in Organized and Constrained Media*, VCH, New York.
5. (a) Breck, D.W. (1974) *Zeolite molecular Sieves*, Wiley, New York. (b) Szostak, R. (1992) *Handbook of Molecular Sieves*, Van Nostrand, New York.
6. (a) Bock, C. R., T. J. Meyer and D. G. Whitten (1974) *J. Am. Chem. Soc.* **96**, 4710. (b) Olmsted III, J., T. J. Meyer (1987), *Phys. Chem.* **91**, 1649. (c) Kalyanasundaram, K. *Coord. Chem. Rev.* **46**, 159.
7. De Wilde, W., G. Peeters and J. H. Lunsford (1980) *J. Phys.*

Chem. **84**, 2306.
8. Vitale, M., N. Castagnola, N. Ortins, J. Brooke, A. Vaidyalingam and P. Dutta (1999) *J. Phys. Chem. B*, **103**, 2408.
9. Borja, M. and P. K. Dutta (1993) *Nature*, **362**, 43.
10. Sykora, M. and J. R. Kincaid (1997) *Nature*, **387**, 162.
11. Castagnola, N., P. Dutta (1998) *J. Phys. Chem. B*, **102**, 1696.
12. Lehn, J-M., J-P. Sauvage and R. Ziessel (1980) *Nouv. J. Chim.* **4**, 355.
13. Das, S. K., P. K. Dutta (1998) *Microporous Mesoporous Mater.* **22**, 475.
14. Lehn, J-M., J-P. Sauvage and R. Ziessel (1981) *Nouv. J. Chim.* **5**, 291.
15. (a) Amouyal, E. and P. Koffi (1985) *J. Photochem.* **29**, 227. (b) Keller, P., A. Moradpour and E. Amouyal (1982) *J. Chem. Soc., Faraday Trans.* **1**, **78**, 3331. (c) Amouyal, E., P. Deller and A. Moradpour (1980) *J. Chem. Soc., Chem. Commun.* 1019.
16. Bein, T (1996) *Chem. Mater.* **8**, 1636.
17. Anderson, M. W., K. S. Pachis, J. Shi and S. W. Carr (1992) *J. Mater. Chem.* **2**, 255.
18. Yonemoto, E. H., Y. I. Kim, R. H. Schmehl, J. O. Wallin, B. A. Shoulders, B.R. Richardson, J. F. Haw and T. E. Mallouk (1994) *J. Am. Chem. Soc.* **116**, 10557.
19. Cooley, L. F., C. E. Headford, L., C. M.Elliott and D. F. Kelley (1988) *J. Am. Chem. Soc.* **110**, 6673.